RSC Advances

ROYAL SOCIETY OF CHEMISTRY

www.rsc.org/advances

Cite this: DOI: 10.1039/c0xx00000x

www.rsc.org/xxxxxx

ARTICLE TYPE

Porous ZnO/Co_3O_4 Heteronanostructures Derived from Nano Coordination Polymers for Enhanced Gas Sorption and Visible Light Photocatalytic Applications

Md. Rakibuddin and Rajakumar Ananthakrishnan*

Received (in XXX, XXX) Xth XXXXXXXXX 20XX, Accepted Xth XXXXXXXXX 20XX
DOI: 10.1039/b000000x

Porous ZnO/Co_3O_4 heteronanostructures are successfully fabricated by a novel one-step solid state conversion of a novel [$(Zn)_x$–$(Co)_{7-x}$ (BDC) (DHS)].$n$$H_2O$ (x = 1, 3, 4, 6)] nano coordination polymers (NCPs). The precursor is prepared by one-pot wet chemical approach at room temperature without any surfactant using dihydroxy salophen ligand and 1,4-benzenedicarboxylic acid as the linkers in presence of zinc (II) acetate and cobalt (II) acetate in DMF solvent. Different weight ratios of the Zn/Co are fabricated in-situ into the hetero-structures during the preparation of the NCPs to tune their physicochemical properties. The produced ZnO/Co_3O_4 nanostructure possesses relatively higher surface area (80-140 m^2/g) and having significant N_2 gas sorption capacity in comparison with reported materials. It is suggested that synergistic effect of each component, higher separation of electron and holes, high surface area and porous structure led to the promising visible light photocatalytic properties. The prepared mixed metal oxides show significant reusability in photocatalysis more than five times without losing their properties. Importantly, the mixed-metal NCPs could be applied as an effective route to generate not only binary oxide, but also ternary or quaternary oxide nanostructures with desired morphology and enhanced physicochemical properties.

Introduction

Now–a-days, the synthesis of heteronanostructures by mixing oxides of dissimilar materials is a centre of attention to improve the physicochemical properties of functional materials.[1] The partial reaction of two oxides creates an interface, which exhibit some new interesting properties due to proximity and diffusion phenomena dominating at the nanoscale range.[2,3] Earlier literature reports the synthesis of various heteronanostructures based on this idea. For example, Fe_2O_3/ZnO hollow nanostructures have been synthesized by Lou et al. to enhance photocatalytic degradation of organic pollutants.[4] In addition, Fe_3O_4/CdS, Mn_2O_3/ZnO, ZnO/SnO, ZnO/CuO, and ZnO/ZnS nanostructures have also been fabricated for different attractive properties.[5–7] Among various metal oxides, n-type ZnO has been recognized as versatile material for various application,[8] while p-type Co_3O_4 is well known for high catalytic activity and Li^{+1} storage capacity.[9,10] It is expected the synergistic combination of these two materials will show the way to enhance physicochemical properties. Previously, ZnO/Co_3O_4 hetero-nanostructures or composites exhibited promising application in gas sensing and catalytic behavior.[8,11]

Department of Chemistry, Environmental Materials & Analytical Chemistry Laboratory, Indian Institute of Technology, Kharagpur 721302, India. E-mail: raja.iitchem@yahoo.com; Fax: +91 3222-282252; Tel: +91 3222-282322

†Electronic supplementary information (ESI) available: Supporting information is available free of charge via internet at hppt://pubs.rsc.org/.

A coordination polymer (CP) is a common term widely used in chemistry and material science, which deals with metal ions linked by coordinated ligands into an infinite array. The formation of these polymers is an automatic self-assemble process.[12,13] There are various types of architectures of CPs that range from simple one-dimensional chains to large crystalline metal–organic frameworks (MOFs). Infinite nano coordination polymers (NCPs) are one type of CPs having dynamic nature and greater level of structural tailorability. These porous NCP materials possess some new and interesting size, shape-dependent physical and chemical properties that are not generally observed in MOF.[14] For this reason, NCPs has been extensively used in many fields, including catalysis, separation, gas storage, drug delivery and energy storage *etc.*[15,16] Recently, thermal decomposition of the NCPs has become a growing field for preparation of metal oxides with improved properties for various applications.[17,18] Nanomaterials with desired morphologies can be achieved by choosing appropriate NCP precursors with special morphologies and under suitable experimental conditions. Calcinations of these materials produce a large amount of gas due to the decomposition of the organic ligands, and a porous structure is formed, which retains the shape of the precursor.[19-21] Binary, ternary or quaternary transition metal oxides are traditionally synthesized in laboratory using high-temperature

reactions that often require several days of heating. This problem can be overcome by using NCP as a precursor. In recent decades, a number of single metal oxides have been synthesized using NCP as the precursors. However, there are very few reports on the synthesis of mixed metal oxides from the NCP precursor.[1,22] Hence, synthesis of ZnO-Co_3O_4 hetero-nanostructures through this facile thermal treatment is demandable.

In the present work, porous ZnO-Co_3O_4 heteronanostructures are synthesized by *in situ* addition of different molar ratios of Zn/Co into a novel mixed-metal NCP as shown in scheme 1. In first step, $[(Zn)_x–(Co)_{7-x}$ (BDC) (DHS)].nH_2O (x = 1, 3, 4, 6)] NCPs or preciously Zn-Co NCP are obtained by one-pot wet chemical approach at room temperature mixing 2,5-dihydroxy salophen (2,5-DHS) ligand with $Zn(OAc)_2$. 2 H_2O, $Co(OAc)_2$.4 H_2O and 1,4-benzene dicarboxylic acid (1,4-H_2BDC) in DMF solvent. Then, the as-prepared mixed metal NCPs are calcined in air to obtain ZnO-Co_3O_4 nanostructures. The NCP has been chosen as a precursor because the facile solid-state diffusion and interfacial contact are improved during calcinations introducing the formation of uniform heterojunction at the nanoscale. Especially, C and N can easily be oxidized into gases and release during calcinations producing a porous nanostructure. Besides, this process is easy for work up, very fast, reaction occurs at a mild temperature and environmentally friendly. More attractively, surface area, gas sorption and photocatalytic properties can easily be tailored by changing metal ions and their stoichiometries. It is important to mention that this method is totally distinct from the other common strategies such as vapor-phase, solution-based and photochemical coating method used for synthesis of ZnO/Co_3O_4 heteronanostructure.[8-11] Although ZnO/Co_3O_4 nanostructures have been widely applied, there is no report for the visible light photocatalytic activity of the material. Interestingly, it is noted that the as-prepared ZnO/Co_3O_4 heterostructures in our method exhibited high surface area, good gas sorption capacity and high photocatalytic activity under visible light.

Experimental

Reagents and materials

The 2,5-dihydroxybenzaldehyde and Zinc acetate dihydrate were obtained from Sigma-Aldrich and SISCO Research Laboratories Pvt. Ltd. (India), respectively and used as received. Cobalt acetate tetra hydrate was obtained from Loba Chemie Pvt. Ltd (India). All other chemicals (solvents) used in this investigation were analytical grade (99.9%). All the solutions were prepared in Distilled/ Millipore water (Milli-Q system).

Preparation of 2,5- dihydroxylated salophen ligands (DHS)

The 2,5-DHS isomer were synthesized according to the literature procedure with slight modifications.[22b] 2,5-dihydroxy benzaldehyde (0.276 g, 2 mmol) was dissolve in ethanol (20 mL), and was added drop-wise to 20 mL ethanol solution of o-phenylenediamine (0.108 g, 1 mmol) and was refluxed at 60 ºC for 30 min. The red colour solution was then evaporated to get dry mass. The mass was dissolved with a small amount of acetone, and then petroleum ether was added to get the product. After filtration of the product, it was dried under open air (yield-0.324 g, 93%).

Preparation of porous hexagonal lump shaped Zn-Co NCPs and corresponding ZnO-Co_3O_4 heteronanostructures

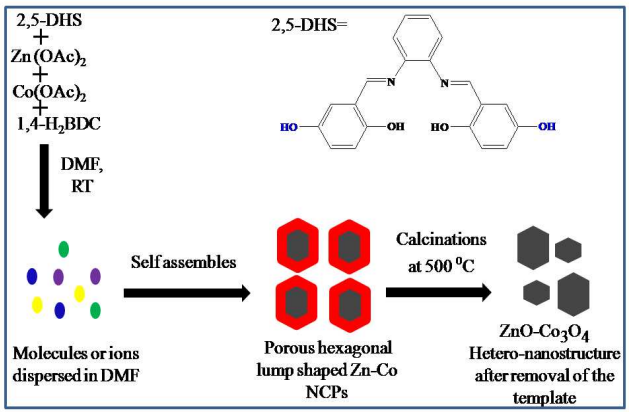

Scheme 1. Schematic representation of the formation of the hexagonal shaped heteronanostructures from the mixed-metal NCP precursors.

The as-prepared 2,5-DHS isomer (23.8 mg, 0.007 mmol) was dissolved in 1 mL of DMF at room temperature. Another solution of $Zn(OAc)_2$. $2H_2O$ and $Co(OAc)_2.4H_2O$ dissolving in a minimum amount of DMF, was added successively to the above prepared solution. Finally, 3 mL DMF solution of H_2BDC (60 mg, 0.035 mmol) was added to the ultimate prepared solution. Within seconds, hexagonal lumps NCPs began to form. Products were centrifuged and washed with acetonitrile two times. The mixed-metal NCPs were then dried at open air. The proportions between $Zn(OAc)_2$ and $Co(OAc)_2$ were varied 6:1, 4:3, 3:4 and 1:6. For 6:1 ratio the concentration of $Zn(OAc)_2$ and $Co(OAc)_2$ used were 0.042 mmol (92 mg) and 0.007 mmol (13.9 mg), respectively keeping the total salt concentration 0.049 mmol, and the same was calculated for other ratios also. The NCP formed from $Zn(OAc)_2$ and $Co(OAc)_2$ was named as Zn-Co NCP (yield ~50%-70%). The Zn-Co NCPs formed from different ratios is named like Zn-Co NCP 61, Zn-Co NCP 43, Zn-Co NCP 34 and Zn-Co NCP 16 for the Zn/Co ratio 6:1, 4:3, 3:4 and 1:6, respectively.

The as-prepared hexagonal lump mixed-metal NCPs were then placed in a conventional furnace and heated at 500 °C for 90 min. The hexagonal shaped ZnO-Co_3O_4 heteronanostructures were generated, and cooled to room temperature. In every case, the loss of weight was ~ 51-57%. The heteronanostructure obtained from corresponding Zn-Co NCP 61, Zn-Co NCP 43, Zn-Co NCP 34 and Zn-Co NCP 16 was named as ZnO-Co_3O_4 61, ZnO-Co_3O_4 43, ZnO-Co_3O_4 34 and ZnO-Co_3O_4 16, respectively.

Photocatalytic Experiments

To measure the photocatalytic activities of the as-synthesized ZnO-Co_3O_4 heteronanostructures, 15 mL of reaction mixture in an aqueous medium containing methylene blue (MB) (1.2×10^{-5} M) and catalytic amount (0.2 g/L) of the samples were taken in a Pyrex glass vessel, and kept in the dark under stirring for 30 min, to maintain adsorption-desorption equilibrium between the dye and the catalyst. After that, the mixture was irradiated under visible light (300 W halogen lamp that contained the aqueous $NaNO_2$ solution (10% w/w) as a light filter through which only

visible light, λ≥420 nm could pass). After a certain regular interval of irradiation time, 2 mL of an aliquot was taken from the reaction mixture, and 2 mL of deionized water was added to the aliquot each time to make the centrifuge easy. The transparent solution thus obtained after centrifuge was preserved in the dark for spectral analysis.

Instrumentation

Fourier Transform InfraRed spectra (FT-IR) were measured with a Perkin-Elmer FT-IR spectrophotometer RXI. Powdered X-ray Diffraction was performed by Bruker APEX-2 diffractometer. Transmission Electron Microscopy (TEM) and High Resolution TEM (HRTEM) were carried out with JEOL JEM2010 electron microscope operating at 200 kV. Energy Dispersive X-ray (EDX) measurement was performed with FEI TECNAI-G2-20S-TWIN (USA). Field Emission Scanning Electron Microscopic (FESEM) image and Elemental Mapping were obtained from a Supra 40, Carl Zeiss instrument. Thermogravimetric Analysis (TGA) was performed on Perkin-Elmer instrument, Pyris Diamond TG/DTA with Al_2O_3 crucible. BET-N_2 sorption isotherms (77K) were performed by using Quantachrome Autosorb-1. The Zn/Co weight percentage in the NCPs was determined by inductively coupled plasma atomic mass spectroscopy (ICP-MS) with a ThermoFisher Scientific ICAP-Q instrument. Prior to analysis, the samples were digested in hot concentrated HNO_3 and H_2O_2 mixture. The X-ray Photoelectron Spectroscopy was carried out by Specs (German). UV-Visible and UV-Visible Diffuse Reflectance Spectra (DRS) was recorded using UV- 1601, Shimadzu and CARY 5000 UV-Vis-NIR spectrophotometer, respectively.

Results and Discussion

Characterization of the Zn-Co NCP derived ZnO-Co_3O_4 heteronanostructure

Zn-Co NCPs were synthesized at room temperature by mixing the corresponding salophen ligand (2,5-DHS) in DMF solution. When the solution of $Zn(OAc)_2$, $2H_2O$ in DMF was added to the previously prepared ligand solution, Zn^{2+} is getting coordinated to the salen pocket to form a light red coloured Zn-metalated salen complex in the reaction. Another DMF solution of $Co(OAc)_2.4H_2O$ when added to the above solution, one equivalent of Co^{+2} replaces the Zn^{2+} from the salen pocket, and another Co^{+2} occupies the carboxylate node position after the addition of H_2BDC to the final solution.[14] This process also has been supported by immediate color change from red to black in the final solution, where hexagonal lump NCPs began to form within seconds in every case. Interestingly, instead of $M(OAc)_2$ when MCl_2, $M(NO_3)_2$ and $M^{II}SO_4$ were used as metal salts, formation of the NCPs did not occur. And when 4-amino benzoic acid was used as the linker instead of 1,4-H_2BDC, NCP formation also did not occur. The above results prove the fact that the formation of the NCP is highly salt and ligand dependent. The Zn-Co NCPs were found to be stable in several solvents such as DMF, DMSO, methanol, and non-polar solvents. However, we have tried to get the crystal of the synthesized polymers dissolving in a suitable solvent by several techniques such as, solvent evaporation, solvent diffusion, slow cooling of the solution, but unfortunately no crystals are obtained.

Firstly, the formation of coordination polymers was verified by infrared (IR) and ^1H NMR spectroscopic techniques (Supporting Information, Fig.S1). As shown in Figure 1a, the nature of the IR spectra of all the NCPs is nearly identical. The coordination of the carboxylate groups of 1,4-H_2BDC to Zn^{2+}/Co^{+2} ions was confirmed by the infrared spectra of the NCPs. The CO stretching frequency shifted to 1575-1579 cm^{-1} from 1686 cm^{-1} for the un-coordinated ligand H_2BDC after the formation of coordination polymers.[23] In all the NCPs, a strong and broad peak at around 3384 cm^{-1} is observed (Supporting Information, Fig. S2) typical for H_2O molecules with hydrogen bonds indicating that H_2O molecules participate in the coordination of Zn^{+2}/Co^{+2} of the NCP structures. The peak of higher intensities at 1371-1385 cm^{-1} in all the Zn-Co NCPs is due to carboxylate stretching frequencies of the ligand, BDC^{2-}. The aromatic -C-H in plane and out of plane bending vibration in all the NCPs are appeared between 950-1248 cm^{-1} and 670-885 cm^{-1}, respectively. Interestingly, all these strong and weak peaks are vanished after calcinations of the NCPs at 500 ^0C for 90 min suggesting the formation of metal oxide heteronanostructures (Figure 1b). A weak band at 1630 cm^{-1} is observed in the ZnO-Co_3O_4 samples, which is due to O–H bending vibration of adsorbed water molecules on the surface of the heteronanostructures.

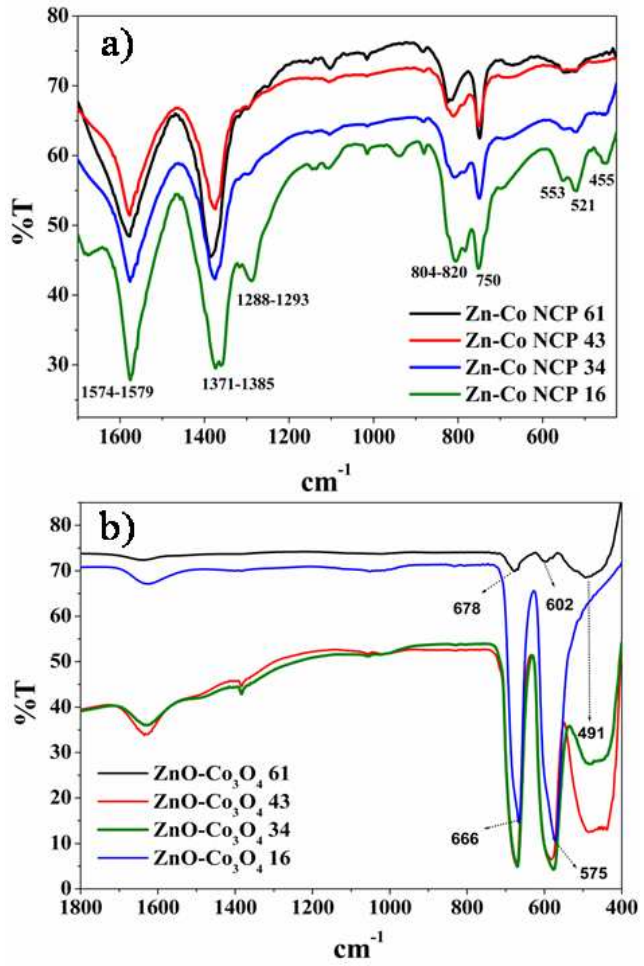

Figure1. FT-IR spectra of the a) Zn-Co NCPs and b) ZnO-Co_3O_4 hetero-nanostructures after calcinations of the Zn-Co NCPs at 500 ºC.

As shown in Figure 1b, the two sharp peaks at 666 cm^{-1} and 575 cm^{-1} in the ZnO-Co_3O_4 16 are shifted from 678 cm^{-1} and 602 cm^{-1} of the ZnO-Co_3O_4 61 are assigned to Co^{+2}–O and Co^{+3}–O vibration of spinal cobalt oxide, respectively.[24] This type of shift indicates an interaction between the two different proportions of one metal oxide with another metal oxide. In addition, the peak at 491 cm^{-1} of the ZnO-Co_3O_4 is due to Zn-O vibration, and the intensity of the peak is slowly decreasing with an increase of Co_3O_4 content in the sample.

The powder X-ray diffraction (PXRD) of the mixed-metal NCPs reveals sharp and intense peak; and hence, indicates crystalline nature of all the NCPs (Figure 2). Though all the NCPs contain same molecular building blocks and same elemental composition, they all are not iso-structural. The PXRD pattern of the NCPs indicates the Zn-Co NCP 34 possesses some different structure than the others. It is noticed that the structure of the NCPs are not changed for all cases by changing the metal ratios, but it is changed at some particular ratio which varied from metal to metal. However, more research is needed to explain the exact reason for this type of changing at that particular ratio of metals as the exact structure of the NCPs is not known at this moment.

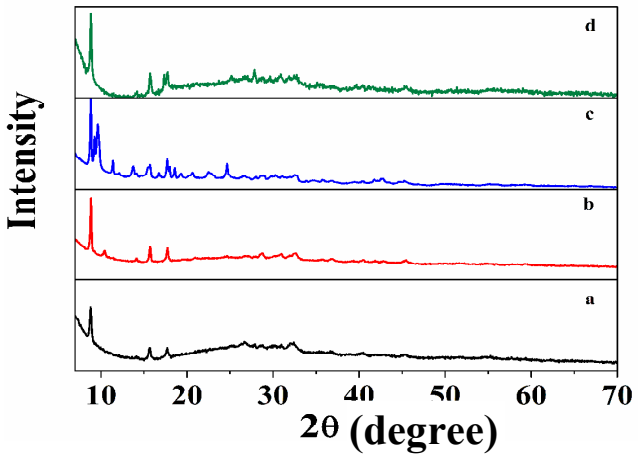

Figure 2. Powder X-ray diffraction pattern of the as-synthesized Zn-Co NCPs: a) Zn-Co NCP 61, b) Zn-Co NCP 43, c) Zn-Co NCP 34, d) Zn-Co NCP 16

Interestingly, an enormous change in the PXRD pattern is observed after heating the NCPs at 500 ^{0}C for 90 min. All the peaks of the NCPs are disappeared and some new sharp and intense diffraction peaks appeared due to the solid state transformation of the NCPs to metal oxide heteronanostructures.

The appearance of new peak in the heteronanostructures suggests that it is highly crystalline in nature (Figure 3). In all heteronanostructures, there are three strong diffraction peaks of the ZnO, which can be ascribed as the pure hexagonal wurtzite phase of ZnO (JCPDS, 36–1451). In Figure 3, the dotted state line shows that the peak intensity of ZnO in the ZnO-Co_3O_4 is decreased, whereas the peak intensity of the Co_3O_4 is increased gradually by changing their concentration. The peak of the Co_3O_4 has been indexed by an asterisk mark in the figure (Fig. 3). The measured peaks at 2θ = 31.13, 36.76, 38.5, 44.8, 55.5, 59.2, 65.26 and 77.4 correspond to (111), (220), (311), (222), (400), (422), (511), (440) and (533) planes of cubic phase of Co_3O_4 crystals, respectively (JCPDS, 42-1467).[25]

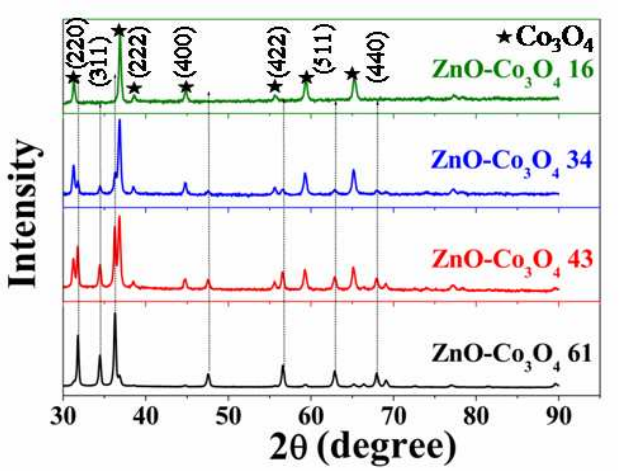

Figure 3. Powder X-ray diffraction pattern of the ZnO-Co_3O_4 hetero-nanostructures synthesized from the Zn-Co NCPs after calcinations at 500 ºC for 90 min.

No peaks of impurities are observed in the XRD pattern, which indicates the formation of single-phase ZnO-Co_3O_4 heteronanostructures in all cases.

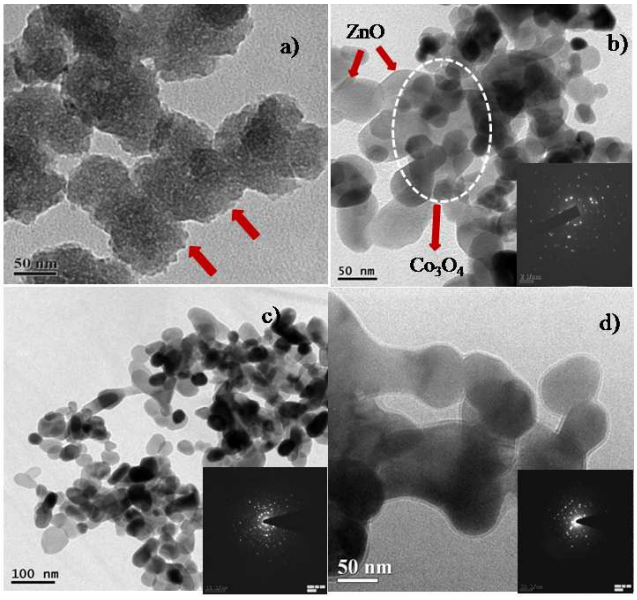

Figure 4. TEM image of the synthesized Zn-Co NCP and ZnO-Co_3O_4 heteronanostructures; a) Zn-Co NCP 61, b) ZnO-Co_3O_4 61,c) ZnO-Co_3O_4 43 and d) ZnO-Co_3O_4 16 (inset corresponding SAED pattern of the heteronanostructures).

In order to take insight into the morphology and size of the Zn-Co NCPs and the as-synthesized ZnO-Co_3O_4 hetero-nanostructures, Transmission Electron Microscopy (TEM) is studied. As shown in Figure 4a, the TEM image of the Zn-Co NCPs reveals the formation of uniform porous particles with a hexagonal lump shape. The TEM image also shows that the average size of the Zn-Co NCP is about 70-100 nm upon changing the Zn/Co ratios (Supporting Information, Fig.S3). However, after the calcinations of the grown Zn-Co NCPs in a conventional furnace, the shape of the produced nanostructures is found to be hexagonal, but the size

is reduced. As shown in Figure 4b, the TEM images clearly show the presence of both individual ZnO and Co_3O_4 in the ZnO-Co_3O_4 heteronanostructures having two different sizes. The TEM images reveal uniform distribution of the particles in the heteronanostructures, where the larger hexagonal shaped particles are of the ZnOs and the smaller hexagonal particles correspond to Co_3O_4. The average size of the ZnOs in the ZnO-Co_3O_4 is found to be 60 nm, whereas the sizes of the Co_3O_4 particles are found to be ~30 nm, which is also supported by the FESEM images (Supporting Information, Fig.S4). Interestingly, the size of the as prepared ZnO-Co_3O_4 nanostructures is found to be less than the corresponding Zn-Co NCPs, which is due to ~50-60% removal of the organic moiety of the NCPs, which is further confirmed by the TGA curve.

When the weight ratio of metal salts (Zn/Co) is varied in the preparation of the NCPs and then the heteronanostructures, there is no significant change in shape of the particles. However, it is noted that the size of the as synthesized nanomaterials is depended on the ligand as well as the nature of metal salts and their proportions used for the preparation of the NCPs.

The Zn-Co NCPs also have been characterized by Energy Dispersive X-ray (EDX) (Supporting Information, Fig.S5). Also the metal ion ratios are verified using Inductive Coupled Plasma Atomic Mass Spectroscopy (ICP-MS) (Fig. 5). The EDX shows the presence of elements C, N, O, Zn and Co in all the NCP structures. The Zn/Co wt.% measured by ICP-MS analysis shows the different loading of Zn and Co from 7.9% to 53.2% on the NCP, depending on the different ratios. These values are well agreed with the loading of metal wt.% measured by EDX analysis and experimentally calculated value.

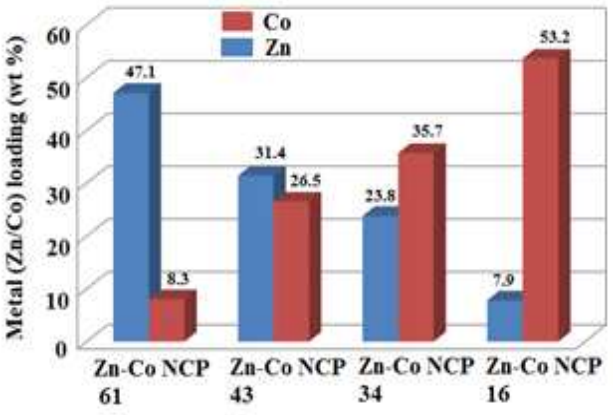

Figure. 5 Metal loading (wt %) in different samples of NCP determined by ICP-MS analysis.

The DRS spectra of the NCPs show broad visible light absorption, and hence the color of the NCPs appears to be black from the two initial colorless precursors (Supporting Information, Fig.S6). After the calcinations of the Zn-Co NCPs at 500 ^{0}C, the EDX shows only the presence of only Zn, O and Co of the ZnO-Co_3O_4 (Supporting Information, Fig.S7). No peaks of C and N are observed in EDX analysis indicating successful removal of the organic template. However, the carbon and copper atom observed in the EDX analysis are due to carbon coated Cu grid used during TEM sample preparation. The EDX analysis of the ZnO-Co_3O_4 clearly exhibits the increase or decrease of peak intensity of the metals (Zn or Co) with changing the proportion of the corresponding salts at the time of preparation of NCPs. Hence, all of these observations suggest successful formation of heteronanostructures from the NCPs while maintaining proper weight ratios.

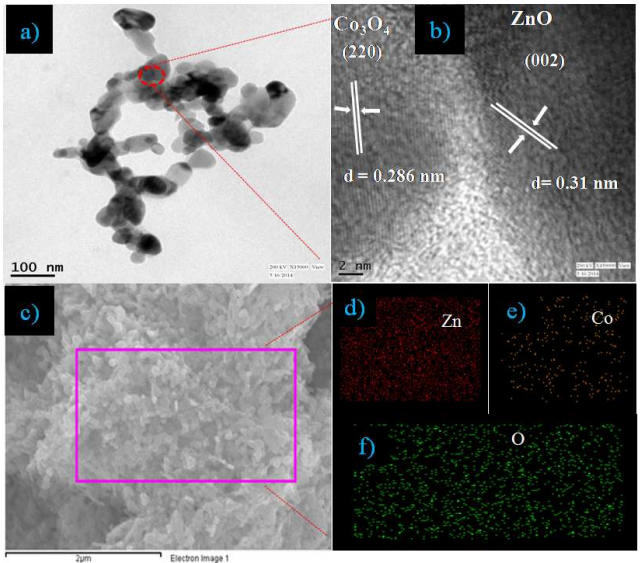

Figure 6 a) Low magnification HRTEM image of the synthesized ZnO-Co_3O_4 16 heteronanostructures, b) High magnification HRTEM image of the ZnO-Co_3O_4 16 showing lattice fringes; c) FESEM images of the ZnO-Co_3O_4 16 and corresponding Elemental Mapping of the Zn, Co, O in the heteronanostructures (d-f).

Figure 6a shows the low magnification High Resolution Transmission Electron Microscopic (HRTEM) image of the prepared heteronanostructures. Figure 6b is a high-resolution image from the red circle containing both larger and smaller particles in Figure 6a, which reveals the heterojunction of the crystalline Co_3O_4 and ZnO crystal lattices in the ZnO-Co_3O_4 16. The HRTEM images clearly exhibits lattice fringes of the prepared materials suggesting highly crystalline nature of the samples, which is also confirmed by the corresponding SAED pattern of the materials in Figure 4. As shown in Figure 6b, the inter-planar distance of 0.286 nm and 0.31 nm is corresponded to the (220) plane of the cubic Co_3O_4 and (002) plane of the hexagonal ZnO.[26] Moreover, a distinguished interface and continuity of lattice fringes between the Co_3O_4 and ZnO, can be observed in Figure 6b, suggesting that the p-n heterojunction is formed between the Co_3O_4 and ZnO in the heteronanostructures. The Figure 6d also shows the elemental area mappings of Zn, O and Co in the selected area of the ZnO-Co_3O_4 61 heteronanostructures of Figure 6c.

The elemental mapping also reveals that the signals are very sensitive to the different proportion of Zn/Co, and clearly show the change (higher or lower) in distribution of the element (Zn/Co) in the sample (Supporting Information, Fig.S8). Hence, the elemental area mapping of the materials indicates successful incorporation of the elements into the heteronanostructures.

X-ray Photoelectron Spectroscopy (XPS) is a powerful technique to investigate the chemical composition, surface property and the interaction of the nanomaterials.

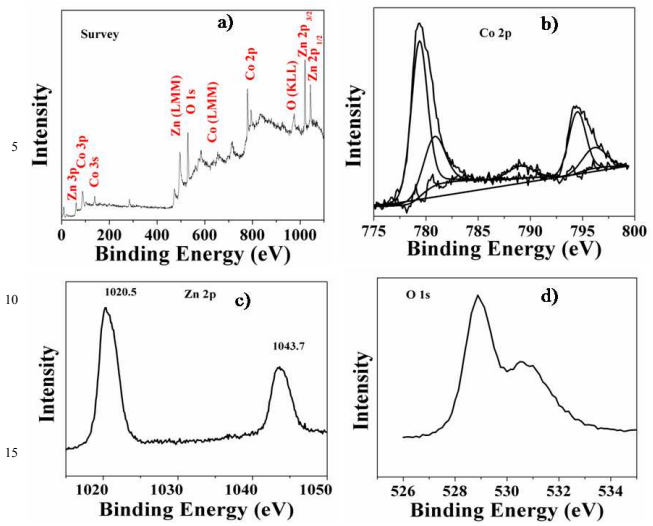

Figure 7. XPS full survey of the synthesized ZnO-Co_3O_4 heteronanostructures, b) High resolution XPS measurement of the Co 2p, c) Zn 2p and d) O 1s of the heterostructures.

Figure 7 shows the full scan and the high resolution XPS spectra of the ZnO-Co_3O_4 hetero-nanostructures. As observed in Figure 7a, the XPS survey indicates the presence of Zn, Co and O in the ZnO-Co_3O_4 samples, and no peaks of other elements are observed, indicating high purity of the synthesized nanostructures, which are also well in agreement with the above XRD and EDX results. The presence of C element could be attributed to the adventitious carbon-based contaminant, and the binding energy at 284.6 eV of the C 1s (not labelled in the figure) is used as the reference for calibration. Subsequently, the Zn 2p high-resolution XPS spectrum of the nanostructures is also analyzed (Figure 7c). For ZnO-Co_3O_4, the Zn $2p_{3/2}$ and Zn $2p_{1/2}$ peak appeared at 1020.6 eV and 1043.6 eV, respectively. The observed spin-orbit splitting of Zn 2p (between Zn $2p_{3/2}$ and Zn $2p_{1/2}$) is about 23 eV, indicating a normal form of Zn^{2+} in the samples.[27] In comparison with pure ZnO (Zn $2p_{3/2}$ at 1020 eV and Zn $2p_{1/2}$ at 1042.3 eV), the Zn 2p peaks of both materials shift to higher energy confirming the interaction and electron transfer between ZnO and Co_3O_4.[28]

As shown in Figure 6b, the high resolution XPS fitting of Co 2p of the ZnO-Co_3O_4 nanostructures shows prominent peaks around at 779.4 eV and 794.5 eV are attributed to Co^{3+} $2p_{3/2}$ and Co^{3+} $2p_{1/2}$ configuration of the Co_3O_4, respectively and the fitting peaks at 780.9, 789.2 and 796.2 eV are due to Co^{2+} peaks of the Co_3O_4.[29] The energy difference between the peak of Co $2p_{3/2}$ and the peak of Co $2p_{1/2}$ is 15.1 eV, which demonstrates the presence of a Co_3O_4 phase.[30] The high resolution XPS spectra of O 1s consist of two peaks (Figure 7 d). A peak at around 529.0 eV is due to oxygen in the Co_3O_4 crystal lattice, which is a characteristic value of cobalt oxide networks, while another peak at around 530.8 eV is due to surface hydroxyl of the obtained nanostructure.[31] The Co 2p peaks in the ZnO-Co_3O_4 is shifted comparatively to lower binding energy than pure Co_3O_4 (781.2 eV for Co^{3+} $2p_{3/2}$).[32] Thus, shifting of the Zn 2p peaks toward the higher binding energy, and the Co 2p peaks to the lower binding energy suggests that there might be Co-O-Zn bonds present at the interface between Co_3O_4 and ZnO in the heterostructures, which is further confirmed by the HRTEM results. Hence, there might exists a strong interaction between the p-type Co_3O_4 and n-type ZnO nanoparticles, which enhances electron transfer in the composites indicating the formation of p-n heterojunctions like structure.

The ability of light absorption is important for the effective excitation and separation of photo induced electron and holes carriers, which are useful factors for the photocatalytic activity of a material. The UV-Vis diffuse reflectance spectra (DRS) of the ZnO-Co_3O_4 heteronanostructures displayed optical absorption capabilities nearly in the entire visible region from 400 to 800 nm (Supporting Information, Fig.S9). The broad-spectrum response indicates that it can be used as good visible light-responsive photocatalysts. The absorbance intensity in the range of 400 nm to 800 nm increases gradually with an increase of Co^{+2} salt concentration with respect to the Zn^{+2} during the preparation of the Zn-Co NCPs. The absorption spectra of ZnO appeared at 365 nm, and the two distinct peaks at 250 to 350 nm and 400 to700 nm wavelength ranges in the ZnO-Co_3O_4 can be assigned to the $O^{2-} \rightarrow Co^{2+}$ and $O^{2-} \rightarrow Co^{3+}$ charge transfer process, respectively.[33] The peaks at 609 and 660 nm of the ZnO-Co_3O_4 became red shifted to 672 and 740 nm with the higher Co ratio, which are the characteristic peak of Co_3O_4.[34] As shown in the Figure, the two absorption edges (Co^{+2} and Co^{+3}) of the ZnO-Co_3O_4 shifted from 516 and 742 nm to 552 nm and 760 nm with the change of proportion of Zn/Co.

Thermal stabilities of the precursor Zn-Co NCPs and synthesized ZnO-Co_3O_4 heteronanostructures

The thermal stabilities of the Zn-Co NCPs and corresponding derived heterostructures were performed by thermogravimetric analysis (TGA) under N_2 atmosphere at the heating rate of 10 ^{0}C min^{-1}. As shown in Figure 8, the Zn-Co NCPs almost maintained the same thermal stability around 500-513 ^{0}C, and is not changed so much upon changing the ratios of the Zn/Co salts. However, different weight loss is observed for Zn-Co NCPs, which varied from 50% to 64%.

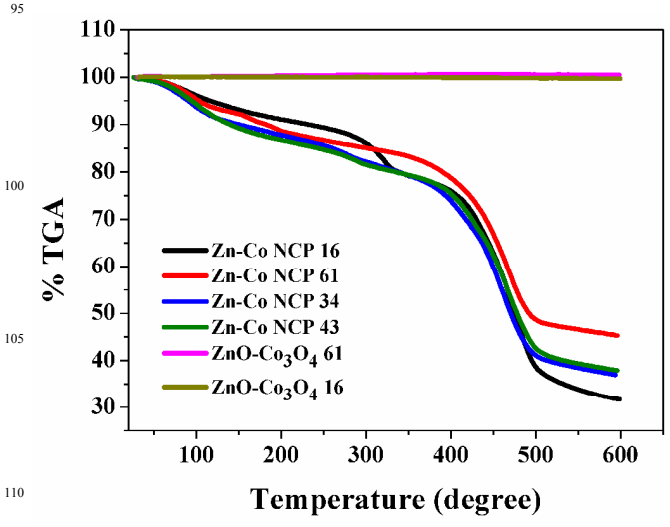

Figure 8. Thermogravimetric Analysis (TGA) curve of the synthesized Zn-Co NCPs and ZnO-Co_3O_4 61 and ZnO-Co_3O_4 16 hetero-nanostructures.

All the Zn-Co NCPs shows its first weight loss around at 100-150 ^{0}C due to removal of water molecules, and the second weight loss around at 300-350 ^{0}C due to removal of H_2BDC unit from the NCPs and finally, the third weight loss around at 500 ^{0}C due to removal of salophen framework from the NCPs.[35] After that, no weight loss is observed indicating successful transformation of the Zn-Co NCPs to ZnO-Co_3O_4 heteronanostructures at that temperature. From the different thermal stabilities and percentage weight loss of the NCP materials, it is demonstrated that the thermal property of NCP is highly dependent on its salt and its proportions, and this is also due to different porosities of the NCPs molecule.[36] Similarly, to observe the thermal stabilities of the synthesized heterostructures, TGA analyses of the samples are carried out under N_2 atmosphere at the same heating rate like the NCPs. The prepared ZnO-Co_3O_4 exhibits no significant weight loss (~ 0.5%) up to 600 ^{0}C indicating high thermal stability of the heterostructures.

Gas sorption property of the as synthesized Zn-Co NCPs and ZnO-Co_3O_4 heteronanostructures

The pore volume, surface area and N_2 gas uptake capacity of the Zn-Co NCP materials and corresponding derived ZnO-Co_3O_4 nanostructures are obtained by Brunauer–Emmett–Teller (BET) measurement. As shown in Figure 9, the BET isotherms of the prepared NCPs and heterostructures follow type III behaviour, which is a weak van der Waals force of attraction between the adsorbate (N_2 gas) and adsorbents (NCPs/heteronanostructures). Thus, the isotherms are reversible in nature as soon as the pressure is released. All the curves do not have any flattish portions, and thus explain the multilayer sorption property of the materials.[37] It is observed that the prepared Zn-Co NCPs exhibits high surface area following the order Zn-Co NCP 61 (225.3 m^2/g) > Zn-Co NCP 43 (202.4 m^2/g) > Zn-Co NCP 16 (189.3 m^2/g) (Supporting Information, Table S1). However, it is noted that the Zn-Co NCP 16 (having highest cobalt ratio) shows the greater pore volume (0.272 cc/g) and gas sorption capacity (295 cc/g) than the other Zn-Co NCPs (Figure 9a). All the Zn-Co NCPs are found to be permanently porous material. It is suggested that the proportions containing higher Zn ratios exhibited higher surface area; hence a particular ratio of Zn/Co is needed to get the optimum surface area and pore size of the NCP material. The Zn-Co NCP derived ZnO-Co_3O_4 hetero-nanostructures also exhibited high surface area, and maintains the previous order as expected like ZnO-Co_3O_4 61 (140.4 m^2/g) > ZnO-Co_3O_4 43 (110.8 m^2/g) > ZnO-Co_3O_4 16 (80.5 m^2/g). All the prepared hetero-nanostructures are also found to be permanently porous, and show significantly higher N_2 gas sorption capacity.

The ZnO-Co_3O_4 61 possesses the highest porosity amongst the heteronanostructures having pore volume 0.552 cc/g and N_2 gas sorption capacity (645 cc/g). Nevertheless, this type of higher porosity of the metal oxide heteronanostructures is not generally observed. Hence, experimental observations indicate that the surface area and pore size of Zn-Co NCPs and synthesized heterostructures are highly depended on salt and their proportions, and hence, the surface area, pore volume and N_2 gas sorption properties can easily be tailored by simply changing the proportions, which will help to choose the best system for desired properties among the different NCPs as well as NCP derived hetero-nanostructures.

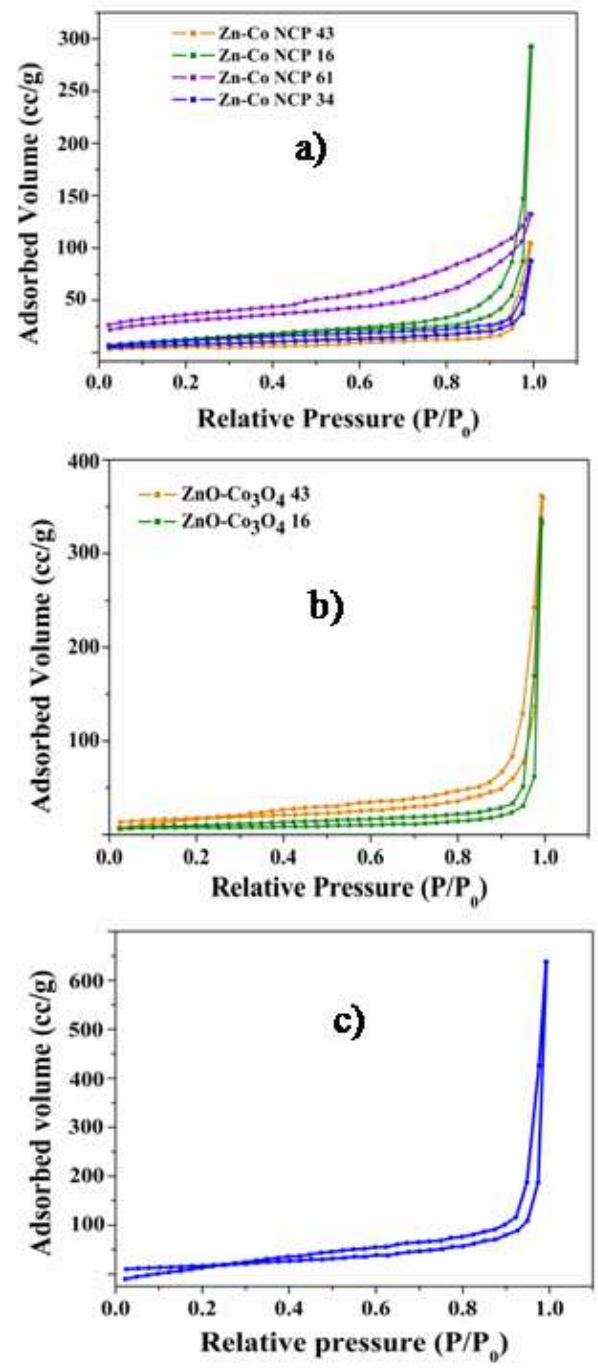

Figure 9. BET-N_2 gas sorption isotherm curve of the synthesized a) Zn-Co NCPs, b) NCP derived ZnO-Co_3O_4 heteronanostructures and c) BET-N2 sorption isotherm of the ZnO-Co_3O_4 61.

Photocatalytic activity of the synthesized ZnO-Co_3O_4 heteronanostructures

The photocatalytic activities of the as-prepared ZnO-Co_3O_4 heteronanostructures are evaluated by measuring the photodegradation of a model dye Methylene Blue (MB) under visible light ($\lambda \geq 420$ nm). MB has its characteristic absorbance maxima at 663 nm, which is used to monitor the photocatalytic degradation. A 15 mL of reaction mixture of MB (1.2×10^{-5} M) in

an aqueous medium containing catalytic amount (0.2 g/L) of the particular ZnO-Co_3O_4 heteronanostructures were taken in a glass vessel, and kept in the dark for 30 min under magnetic stirring condition for any adsorption-desorption equilibrium, and after that it was irradiated under light. The photocatalytic activity is checked for all the heteronanostructure materials.

Figure 10a shows UV-visible absorption spectra of the degradation of MB dye by the different ZnO-Co_3O_4 catalyst under visible light and the kinetic plot (C_t/C_0 *vs* time) of the degradation under various conditions is shown in Figure 10b. MB itself does not decompose under the irradiation of visible light. Similarly, ZnO also does not have any photocatalytic performance under the visible light as it does not absorb visible light. It is noted that when the photodegradation of MB dye is carried out in presence of ZnO-Co_3O_4 61 catalyst under dark, no significant photodegradation (3-4%) of MB is observed. Hence, this control experiment proves the essentiality of the visible light in the photocatalytic process. However, in presence of the ZnO-Co_3O_4 61 catalyst under visible light, the degradation of MB is reached up to 85% in 5 h. Interestingly, the photocatalytic activity is significantly decreased to 50% in 5 h when ZnO-Co_3O_4 16 is employed as the photocatalyst, whereas the ZnO-Co_3O_4 43 catalyst exhibit moderate photocatalytic activity (70%) (Supporting Information, Fig.S10). The ZnO-Co_3O_4 34 catalyst exhibited poor photocatalytic activity (54%) similarly like ZnO-Co_3O_4 16. However, the huge change in photocatalytic activity can be attributed by the different factors such as, surface area, porosities and p-n heterojunction of the heteronanostructures. As the BET surface area measurement shows the catalyst, ZnO-Co_3O_4 61 possessed relatively higher surface area and pore size than that of the ZnO-Co_3O_4 43 and ZnO-Co_3O_4 16; hence, it shows higher activity than the others. This is due to the adsorption of the dye molecule on the porous catalyst surface, so when the light is irradiated the adsorbed dye fully degraded. The enhanced photocatalytic activity of the ZnO-Co_3O_4 heteronanostructures for the degradation of MB could be ascribed by also the formation of p-n heterojunctions like structure in the hetero-nanostructures, which enhances the separation of electron-holes at the interface of the heterojunction of the ZnO and Co_3O_4. The formation of the heterojunction is also supported by the HRTEM (Figure 6b) and XPS studies. All the ZnO-Co_3O_4 photocatalyst follow pseudo-first order rate kinetics, and the ZnO-Co_3O_4 61 exhibits 2.5 times higher rate constant (k = 5.8 × 10^{-3} min^{-1}) value than the ZnO-Co_3O_4 16 catalyst (k = 2.2 × 10^{-3} min^{-1}) (Supporting Informations, Fig.S10c). It is noted that the photocatalytic activity of the ZnO-Co_3O_4 61 is superior to some other ZnO-based nanostructures reported previously.[38-42]

The effect of dye concentration on the photodegradation is also examined. For this, we have chosen the ZnO-Co_3O_4 61 catalyst having highest photocatalytic activity, and the concentration of dye is varied from 1.2 x 10^{-5} $molL^{-1}$ to 3.6 x 10^{-5} $molL^{-1}$. It is observed that with increase in dye concentration from 1.2 x 10^{-5} $molL^{-1}$ to 3.6 x 10^{-5} $molL^{-1}$ the photodegradation is decreased to 60% from 90% for the ZnO-Co_3O_4 61 catalyst (supporting information, Fig.S11). A comparative study also has been carried out between the Zn-Co NCPs and ZnO-Co_3O_4, which reveals Zn-Co NCPs has very low activity in comparison with ZnO-Co_3O_4 (supporting information, Fig.S12). As the heterogeneous catalyst

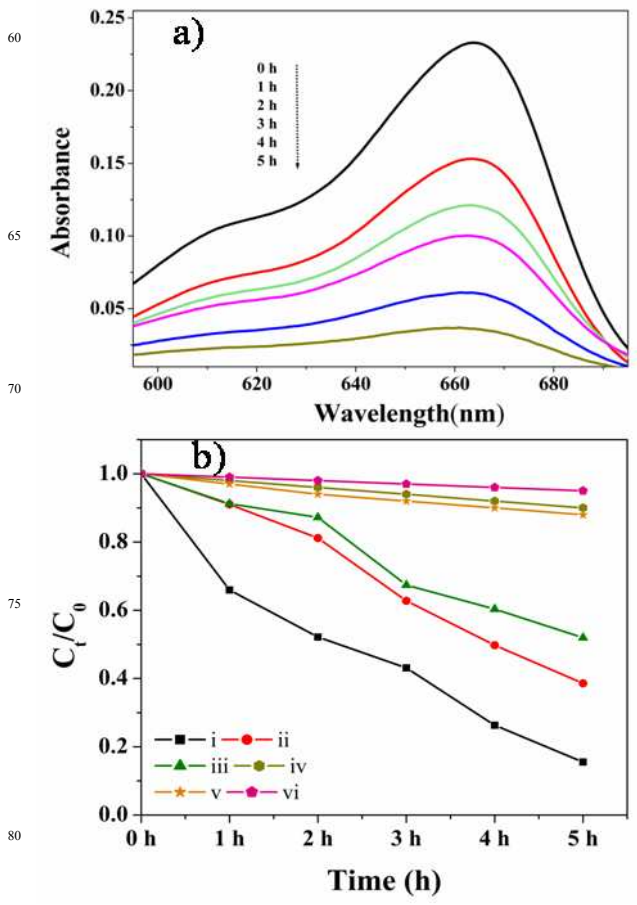

Fig ure 10 a) UV-Visible absorption spectra of the degradation of MB dye in presence of ZnO-Co_3O_4 61 and b) kinetic plots (Ct/C0 vs time) for the visible light (λ ≥ 420 nm) photocatalytic decomposition of MB in the presence of different hetero-nanostructures: i) ZnO-Co_3O_4 61, ii) ZnO-Co_3O_4 43, iii) ZnO-Co_3O_4 16, iv) only MB dye under visible light irradiation, v) only ZnO under visible light irradiation and vi) ZnO-Co_3O_4 61catalyst under dark.

can be recycled, the reusability of the prepared catalysts i.e. heteronanostructures, haven been experimented in our study and reported (Supporting Information, Fig. S13). It is noticed that the prepared catalyst can be easily recycled several times without any major loss of photocatalytic activity (2-3% loss of activity after four cycles). However, more decrease in photocatalytic activity is observed after fifth cycles due to photo corrosion of ZnO and Co_3O_4 nanostructures. Overall, the present photocatalytic system is stable enough at room temperature.

Electron-hole scavenger study and probable mechanistic pathways of the reaction

Inorder to gain more in-depth knowledge about the photocatalytic mechanism, an electron and hole scavenger study is carried out. The hydroxyl radical (OH^-) and superoxide radical ion (O_2^-) are reactive intermediates in the photocatalysis process, and are generated during the reaction of electrons and holes with H_2O separately. However, the main reactive species are electrons and holes. To prove this, scavenging experiments were carried out in presence of $AgNO_3$ and ammonium oxalate, which are good electron and hole scavengers.[43] Electron and hole scavengers

(10^{-3} M) are introduced prior to the addition of the catalyst to the solution of MB.

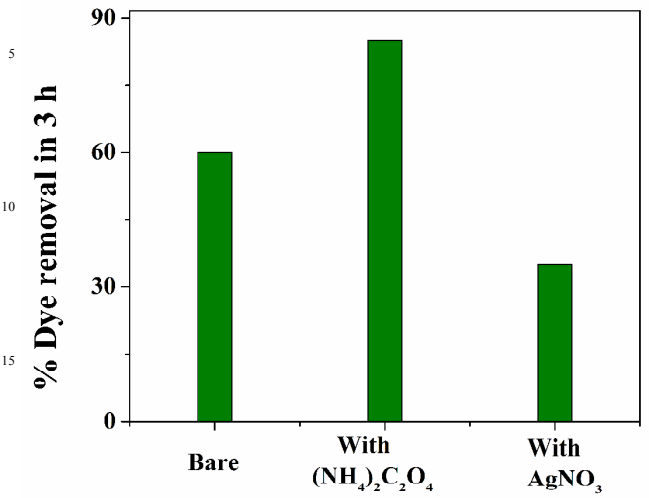

Figure 11. Bar diagram representation of electron-hole scavenger study showing the dye removal efficiency of the ZnO-Co_3O_4 61in 3 h under visible light in the presence of ammonium oxalate and silver nitrate.

Figure 11 shows a bar diagram to represent the degradation of MB by the ZnO-Co_3O_4 61 in the presence of electron scavenger, $AgNO_3$ and hole scavenger, ammonium oxalate. The bare ZnO-Co_3O_4 61 shows 60% dye removal efficiency in 3 h under visible light. The immobilization of the Ag^+ ions on the catalyst surface hinder the adsorption of cationic Methylene Blue[44] as a result only 36% of the dye is degraded under the same condition by the ZnO-Co_3O_4 61. However, in the presence of ammonium oxalate the rate of the degradation is increased to 85% at the same condition for the ZnO-Co_3O_4 61. This is due to the scavenging of the holes, the probability of recombination of electron and holes diminishes and the rate of reaction increases. Hence, electrons and holes are the most powerful species that actively take part in photocatalysis. Successive electron transfer from the conduction band (CB) of Co_3O_4 to the CB of ZnO leads to the higher electron-hole separation[45] Based on the results and literature report, a plausible mechanistic pathway of the present photocatalytic system in our experiment is shown as follows:

$$ZnO\text{-}Co_3O_4 + h\nu \xrightarrow{\lambda \geq 420\ nm} Co_3O_4\,(h^+) / ZnO\,(e^-)$$

$$ZnO\,(e^-) + O_2 \longrightarrow O_2^{\cdot -}$$

$$O_2^{\cdot -} + H_2O \longrightarrow H_2O_2 + OH^- \qquad (1)$$

$$H_2O_2 \longrightarrow OH^-$$

$$OH^- + \text{Organic dye} \longrightarrow CO_2 + H_2O$$

$$Co_3O_4\,(h^+) + H_2O \longrightarrow OH^- \qquad (2)$$

$$OH^- + \text{Organic dye} \longrightarrow CO_2 + H_2O$$

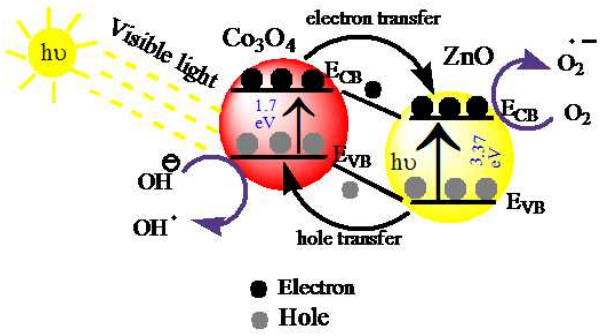

Figure 12. Schematic diagram showing the energy band structure and Electron–hole pair separation in the ZnO-Co_3O_4 heterojunction.

The ZnO-Co_3O_4 heteronanostructure upon irradiation of a particular light generates electron–hole pairs on the surface of Co_3O_4 and absorbing the necessary energy, electrons from the valence band (VB) of Co_3O_4 excited across the conduction band (CB). As the conduction band energy of ZnO is lower than Co_3O_4, the electrons from the CB of Co_3O_4 transfer to the CB of ZnO through the heterojunction (Fig. 12).

The conduction band electrons of ZnO then react with dissolved oxygen forming a superoxide radical, which again reacts with water to give a hydroxyl radical.[46] The produced hydroxyl radical then degrades the organic dye molecule (eqn. 1). Again, the holes of the VB of MO react with water molecules to generate hydroxyl radicals, which can further decompose the organic dye (eqn. 2).

Conclusions

In summary, porous ZnO-Co_3O_4 heteronanostructures were successfully prepared by thermal decomposition of novel $[(Zn)_x (Co)_{7-x} [C_{60} H_{32} N_2 O_{24}].nH_2O$ (x = 1, 3, 4, 6)] NCPs precursor template. The mixed-metal NCPs have been utilized as a tool to tune the surface area, porosity and size of the heteronanostructures, which are useful factors for many physicochemical properties. The ZnO-Co_3O_4 61 hetero-nanostructures exhibited relatively high surface area (140.4 m^2/g), pore volume (0.552 cc/g) and N_2 gas sorption capacity (645 cc/g). Moreover, ZnO-Co_3O_4 heteronanostructures show high visible light photocatalytic ability, which can be attributed to the high surface area, greater pore volume and higher separation of electron and holes in the heterojunction.

The prepared heterogeneous ZnO-Co_3O_4 heteronanostructures photocatalyst is stable enough, which would greatly promote their industrial application in eliminating organic pollutants from wastewater. We believe that these active porous ZnO-Co_3O_4 hetero-nanostructures could serve as a potential candidate for other applications, such as artificial photosynthesis and lithium-ion batteries. Hence, it is expected that library of porous hetero-nanostructures with enhanced properties could be fabricated by using these mixed-metal NCPs as a precursor. Interestingly, it is tested that the synthesis of heteronanostructures is not only limited to binary, but also possible to fabricate ternary and quaternary systems by the facile in-situ addition of different salts during the preparation of the NCP precursors.

Acknowledgements

Authors are thankful to the CRF-IIT Kharagpur for TEM, HRTEM, FESEM, EDX analysis and DST-FIST for powder X-ray (at Department of Chemistry) and XPS (at Department of Physics). The author, MR, thanks the CSIR for research fellowship and RA thanks SRIC, IIT Kharagpur for SDGRI funding (NPA). Also authors are thankful to Prof. K. Biradha, Department of Chemistry (for BET analysis) and Prof. D. Upadhyay, Department of Geology and Geophysics (for ICP-MS analysis), IIT Kharagpur.

Notes and references

1 L. Hu, P. Zhang, Y. Sun, S. Bao and Q. Chen, *ChemPhysChem* 2013, **14**, 3953 – 3959.
2 A. Brinkman, M. Huijben, M. V. Zalk, J. Huijben, U. Zeitler, J. C. Maan, W. G. V. Wiel, G. Rijnders, D. H. A. Blank and H. Hilgenkamp, *Nat. Mater*. 2007, **6**, 493 –496.
3 F. Y. Bruno, J. G. Barriocal, M. Torija, A. Rivera, Z. Sefrioui, C. Leighton, C. Leon and J. Santamaria, *Appl. Phys. Lett.* 2008, **92**, 082106.
4 Y. Liu, L. Yu, Y. Hu, C. F. Guo, F. M. Zhang and X. W. (David) Lou, *Nanoscale* 2012, **4**, 183 –187.
5 J. S. Chen, C. P. Chen, J. Liu, R. Xu, S. Z. Qiao and X. W. Lou, *Chem. Commun.* 2011, **47**, 2631 –2633.
6 X. W. Liu, Z. Fang, X. J. Zhang, W. Zhang, X. W. Wei and B. Y. Geng, *Cryst. Growth Des*. 2009, **9**, 197– 202.
7 Y. Hu, H. H. Qian, Y. Liu, G. H. Du, F. M. Zhang, L. B. Wang and X. Hu, *CrystEngComm* 2011, **13**, 3438 –3443.
8 D. Bekermann, A. Gasparotto, D. Barreca, C. Maccato, E. Comini, C. Sada, G. Sberveglieri, A. Devi and R. A. Fischer, *ACS Appl. Mater. Interfaces* 2012, **4**, 928– 934.
9 X. W. Xie, Y. Li, Z. Q. Liu, M. Haruta and W. J. Shen, *Nature* 2009, **458**, 746 – 749.
10 X. L. Xiao, X. F. Liu, H. Zhao, D. F. Chen, F. Z. Liu, J. H. Xiang, Z. B. Hu and Y. D. Li, *Adv. Mater.* 2012, **24**, 5762 –5766.
11 C. W. Na, H. S. Woo, I. D. Kim and J. H. Lee, *Chem. Commun.* 2011, **47**, 5148 – 5150.
12 A.Y. Robin and K.M. Fromm, *Coord. Chem. Rev.* 2006, **250**, 2127-2157.
13 M.L. Hu, A. Morsali and L. Aboutorabi, *Coord. Chem. Rev.* 2011, **255**, 2821-2859.
14 A. M. Spokoyny, D. Kim, A. Sumrein and C. A. Mirkin, *Chem. Soc. Rev*. 2009, **38**, 1218–1227.
15 F. M. Tabellion, S. R. Seidel, A. M. Arif and P. J. Stang, *J. Am. Chem. Soc.* 2001, **123**, 7740-7741.
16 O. M. Yaghi, M. O'Keeffe, N. W. Ockwig, H. K. Chae, M. Eddaoudi, and J. Kim, *Nature* 2003, **423**, 705-714.
17 W.L. Leong and J.J. Vittal, *Chem. Rev.* 2010, **111**, 688-764.
18 J.J. Vittal and M.T. Ng, *Acc. Chem. Res.* 2006, **39**, 869-877.
19 H. Pang, F. Gao, Q. Chen, R. Liu and Q. Lu, *Dalton Trans*. 2012, **41**, 5862–5868.
20 C. C. Li, L. Mei, L. B. Chen, Q. H. Li and T. H. Wang, *J. Mater. Chem*. 2012, **22**, 4982–4988.
21 D. Su, H. S. Kim, W. S. Kim and G. X. Wang, *Chem. Eur. J.* 2012, **18**, 8224–8229.
22 P. Mahata, G. Sankar, G. Madras and S. Natarajan, *Chem. Commun.* 2005, 5787–5789; b) R. Kitaura, G. Onoyama, H. Sakamoto, R. Matsuda, S. Noro and S. Kitagawa, *Angew. Chem. Int. Ed*. 2004, **43**, 2684-2687.
23 S. Jung, W. Cho, H. J. Lee and M. Oh, *Angew. Chem. Int. Ed*. 2009, **48**, 1459-1462.
24 T. He, D. Chen, X. Jiao and Y. Wang, *Adv. Mater.* 2006, **18**, 1078-1082.
25 H. Nguyen and S. A. El-Safty, *J. Phys. Chem. C* 2011, **115**, 8466–8474.
26 C. W. Na, H. S. Woo, I. D. Kim and J. H Lee, *Chem. Commun*. 2011, **47**, 5148–5150.
27 P. Gao, Z. Liu and D. D. Sun, *J. Mater. Chem. A* 2013, **1**, 14262-14269.
28 Q. Zhang, C. Tian, A. Wu, T. Tan, L. Sun, L. Wang and H. Fu, *J. Mater. Chem.* 2012, **22**, 11778–11784.
29 C. Yuan, J. Li, L. Hou, L. Yang, L. Shen and X. Zhang, *J. Mater. Chem.* 2012, **22**, 16084-16090.
30 C. Yuan, L. Yang, L. Hou, J. Li, Y. Sun, X. Zhang, L. Shen, X. Lu, S. Xiong and X. W. D. Lou, *Adv. Funct. Mater*. 2012, **22**, 2560-2566.
31 H. Huang, W. Zhu, X. Tao, Y. Xia, Z. Yu, J. Fang, Y. Gan and W. Zhang, *ACS Appl. Mater. Interfaces* 2012, **4**, 5974-5980.
32 W. Chu, P. A. Chernavskii, L. Gengembre, G. A. Pankina, P. Fongarland and A. Y. Khodakov, *J. Catal.* 2007, **252**, 215–230.
33 T. He, D. R. Chen, X. L. Jiao, Y. L. Wang and Y. Z. Duan, *Chem. Mater.* 2005, **17**, 4023–4030.
34 D. Barreca, C. Massignan, S. Daolio, M. Fabrizio, C. Piccirillo, L. Armelao and E. Tondello, *Chem. Mater*. 2001, **13**, 588-593.
35 W. Chen, J. Y. Wang, C. Chen, Q. Yue, H. M. Yuan, J. S. Chen and S. N. Wang, *Inorg. Chem*. 2003, **42**, 944-946.
36 W. Cho, H. J. Lee and M. Oh, *J. Am. Chem. Soc*. 2008, **130**, 16943-16946.
37 Y. Chen, K. Munechika and D. S. Ginger, *Nano Lett*. 2007, **7**, 690-696.
38 M. Lee and K. Yong, *Nanotechnology* 2012, **23**, 194014.
39 G. Fan, W. Sun, H. Wang and F. Li, *Chem. Eng. J.* 2011, **174**, 467-474.
40 M. T. Uddin, Y. Nicolas, C. Olivier, T. Toupance, L. Servant, M. M. Müller, H-J. Kleebe, J. Ziegler and W. Jaegermann, *Inorg. Chem.* 2012, **51**, 7764-7773.
41 C. Ren, B.Yang, M. Wu, J. Xu, Z. Fu, Y. lv, T. Guo, Y. Zhao and C. Zhu, *J. Hazard. Mater*. 2010, **182**, 123–129.
42 L. Sun, D. Zhao, Z. Song, C. Shan, Z. Zhang, B. Li and D. Shen, *J.Colloid. Interface Sci*. 2011, **363**, 175–181.
43 A. Kudo, K. Ueda, H. Kato and I. Mikami, *Catal. Lett.* 1998, **53**, 229-230.
44 M. Basu, N. Garga and A. K. Ganguli, *J. Mater. Chem. A* 2014, **2**, 7517–7525.
45 J. C. Dai, X. T. Wu, Z. Y. Fu, C. P. Cui, S. M. Hu, W. X. Du, L. M. Wu, H. H. Zhang and R. Q. Sun, *Inorg. Chem.* 2002, **41**, 1391-1397.
46 T. J. Liu, Q. Wang and P. Jiang, *RSC Adv*. 2013, **3**, 12662-12670.

Graphical Abstract

Porous ZnO/Co_3O_4 Heteronanostructures Derived from Nano Coordination Polymers for Enhanced Gas Sorption and Visible Light Photocatalytic Applications

*Md.Rakibuddin and Rajakumar Ananthakrishnan**

Department of Chemistry, Indian Institute of Technology, Kharagpur 721 302, India.